THE STUDY ABOUT CLOUD OF POINTS RECONSTRUCTION WITH THE FRAMEWORK OF MESHFREE METHOD FOR VISCOUS FLOWS

Y. D. Wang

Shanghai Institute of Space Propulsion
Shanghai, China

Shanghai Engineering Research Center of Space Engine
Shanghai, China

School of Energy and Power Engineering
Nanjing University of Science and Technology
Nanjing, China

Y. Jing **J. Dai** **Q. G. Lin**

Shanghai Institute of Space Propulsion
Shanghai, China

Shanghai Engineering Research Center of Space Engine
Shanghai, China

X. W. Cai

China Ship Scientific Research Center
National Key Laboratory of Science and Technology on Hydrodynamic
Wuxi, China

X. J. Ma

Shanghai Xinli Power Equipment Research Institute
Shanghai, China

D. F. Ren **J. J. Tan***

School of Energy and Power Engineering
Nanjing University of Science and Technology
Nanjing, China

ABSTRACT

A new method, called Cloud of Points (COP) Reconstruction, is proposed in the present work to extend the meshfree method to simulate viscous flows. With the characters of viscous flows, the anisotropic COP structure is distributed in boundary layer. The proposed method can improve the anisotropic COP structure to isotropic COP structure and reduce the condition number of the least square coefficient matrix for conventional meshfree method. The values of the new reconstructed points are calculated by the Lagrange interpolation. The accuracy and the robustness of the presented meshfree solver are demonstrated on a number of standard test cases, including the functions with analytical gradients and the viscous flows past NACA0012 airfoil. The comparison of the simulation results with the experimental data and other numerical simulation data are also investigated.

Keywords: Meshfree method, Cloud of Points (COP) Reconstruction, Viscous flow, Moving least square.

1. INTRODUCTION

The meshfree ('meshless', 'gridless', or 'gridfree') method was first formally proposed by Lucy [1], which was successfully applied in the field of astrophysics. Different from traditional mesh-based method, meshfree

* Corresponding author (dlxyjx@mail.njust.edu.cn)

DOI : 10.1017/jmech.2017.35
Copyright © 2017 The Society of Theoretical and Applied Mechanics
https://doi.org/10.1017/jmech.2017.35 Published online by Cambridge University Press

method is a numerical algorithm that only needs nodes information and does not need to connect nodes into mesh cells to divide the computational domain. So the meshfree method can bring the advantage of flexible point distribution. These meshfree methods are summarized in excellent works by Liu [2] and Liu and Gu [3]. They have classified the gridless methods into three major categories: Finite integral representation methods (such as Smoothed Particle Hydrodynamics (SPH)); Finite series representation methods (such as Moving least squares (MLS) methods); Finite differential representation methods (such as Finite difference method on regular grids). The least squares based meshfree method is first presented by T. Liszkaand J. Orkisz [4] in solid mechanics. Although the meshfree method has achieved great success in the field of solid mechanic, it starts a little later in the field of Computational Fluid Dynamics (CFD). The meshfree method was first introduced into the CFD by Batina [5], who developed an explicit least square meshfree algorithm based on the minimal surface approximation. Now the least square meshfree is widely used in computational fluid dynamics [6-11]. Recently, a new mshfree CFD solver based on gradient smoothing method (GSM) [12, 13] has been developed by Liu and his colleagues by combining the major features of the standard FVM and some meshfree techniques.

A lot of effort has been spent on meshfless method with inviscid flows or low Reynolds number flows since the meshfree method was introduced into the CFD field, but the research progress of using meshfree method with turbulence model to solve the Navier-Stokes equations is still not obvious. The main reason is that to accurately calculate the boundary layer, the size of the minimum space in a direction normal to the boundary layer should be adequately small. In this situation, the cloud of points near the body surface will be high anisotropic, as a result, the condition coefficient number of the least square coefficient matrix is much larger than 1, even as high as 106, thus it will be difficult to use the least square method to accurately calculate the spatial derivative. To solve this problem and extend the meshfree method to high Reynolds number turbulent flows, only a few meshfree method approaches have been proposed.

Munikrishna and Balakrishnan [14], Namvar and Jahangirian [15] used the Green-Gauss formula instead of the least square method to solve the spatial derivatives in viscous layer with different turbulence models. Su, Yamamoto and Nakahashi [16] study the high Reynolds number flow using meshfree method from the aspects of theory and numerical. Katz and Jameson [17] extended the meshfree method to the discretization of the viscous flux terms of the Navier-Stokes equations. And they used this viscous meshfree scheme as a means of communicating to embed within an overset grid context. Kennett *et al.* [18] developed a fully implicit meshfless method with one equation of Spalart-Allmaras turbulence model to solve several viscous flows.

In the present paper, a new meshfree method, called the Cloud of Points Reconstruction, is proposed to reduce the condition number of the least square coefficient matrix and the the anisotropic cloud of points structure can be repaired to nearly isotropic. The meshfree method can be extended to simulate high Reynolds number viscous flows.

2. GOVERNING EQUATIONS

The two-dimensional, compressible Navier-Stokes (N-S) equations to be solved in the present paper can be expressed in the following form:

$$\frac{\partial Q}{\partial t}+\frac{\partial f}{\partial x}+\frac{\partial g}{\partial y}-\frac{\partial F}{\partial x}-\frac{\partial G}{\partial y}=0 \tag{1}$$

Where

$$Q=\begin{pmatrix}\rho\\ \rho u\\ \rho v\\ \rho e\end{pmatrix},\quad f=\begin{pmatrix}\rho u\\ \rho uu+p\\ \rho uv\\ (\rho e+p)u\end{pmatrix},\quad g=\begin{pmatrix}\rho v\\ \rho uv\\ \rho vv+p\\ (\rho e+p)v\end{pmatrix},$$

$$F=\begin{pmatrix}0\\ \tau_{xx}\\ \tau_{xy}\\ u\tau_{xx}+v\tau_{xy}-q_x\end{pmatrix},\quad G=\begin{pmatrix}0\\ \tau_{yx}\\ \tau_{yy}\\ u\tau_{yx}+v\tau_{yy}-q_y\end{pmatrix} \tag{2}$$

In equation 2, u and v represent velocity components in the x and y directions. ρ, e and p are the density, total energy and pressure, respectively. τ is the molecular stress, q is the heat flux term, and

$$e=\frac{p}{\rho(\gamma-1)}+\frac{(u^2+v^2)}{2} \tag{3}$$

$$\tau_{xx}=2\frac{Ma_\infty}{\mathrm{Re}}(\mu_l+\mu_t)\left(\frac{\partial u}{\partial x}-\frac{1}{3}\left(\frac{\partial u}{\partial x}+\frac{\partial v}{\partial y}\right)\right) \tag{4}$$

$$\tau_{yy}=2\frac{Ma_\infty}{\mathrm{Re}}(\mu_l+\mu_t)\left(\frac{\partial v}{\partial y}-\frac{1}{3}\left(\frac{\partial u}{\partial x}+\frac{\partial v}{\partial y}\right)\right) \tag{5}$$

$$\tau_{xy}=\tau_{yx}=\frac{Ma_\infty}{\mathrm{Re}}(\mu_l+\mu_t)\left(\frac{\partial u}{\partial y}+\frac{\partial v}{\partial x}\right) \tag{6}$$

$$q_x=-\frac{\gamma}{\gamma-1}\frac{Ma_\infty}{\mathrm{Re}}\left(\frac{\mu_l}{\mathrm{Pr}_l}+\frac{\mu_t}{\mathrm{Pr}_t}\right)\frac{\partial(p/\rho)}{\partial x} \tag{7}$$

$$q_y=-\frac{\gamma}{\gamma-1}\frac{Ma_\infty}{\mathrm{Re}}\left(\frac{\mu_l}{\mathrm{Pr}_l}+\frac{\mu_t}{\mathrm{Pr}_t}\right)\frac{\partial(p/\rho)}{\partial y} \tag{8}$$

With the prefect gas assumption, the pressure can be calculated from the equation of state:

$$p=(\gamma-1)\left[\rho e-\frac{1}{2}\rho(u^2+v^2)\right] \tag{9}$$

Where λ denotes the ratio of specific heats of fluid and typically taken as 1.4 for air.

https://doi.org/10.1017/jmech.2017.35 Published online by Cambridge University Press

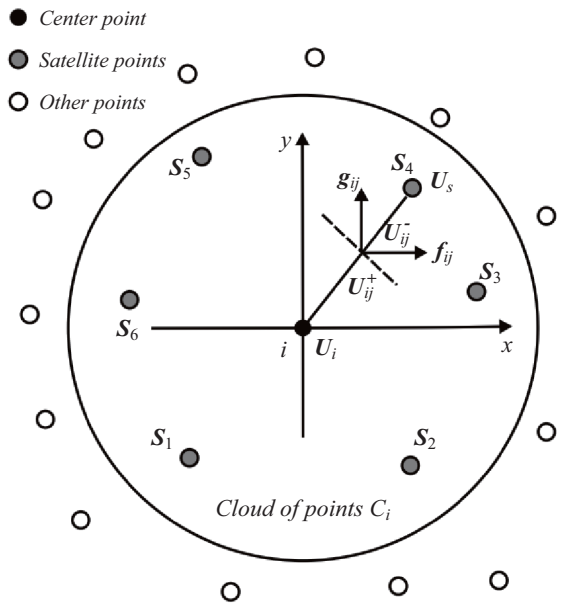


Fig. 1 The illustration of cloud of points and fluxes split.

3. NUMERICAL ALGORITHM

3.1 Spatial Discretization

In essence, using meshfree method to solve the expression (1) in the present work is to use the corresponding numerical scheme to obtain the fluxes and then use the moving least square meshfree method to approximate the spatial derivatives of the fluxes. The moving least square meshfree method, which is a non-integral type meshfree method, only requires the information of the surrounding points at any given point, which is called "clouds of points", to solve the spatial derivatives, and this method has become one of the most widely used meshfree methods in CFD areas currently.

Unlike the grid-based method, the stencil of a meshfree method does not have any particular topology, as show in Fig. 1. The spatial derivatives of point i is calculated by the weighted least square method, which is based on Taylor formulation in the present paper. Assuming that arbitrary function $\phi(x,y)$ represented by "cloud" C_i, and can be written as:

$$\phi_j = \phi_i + (x_j - x_i)\frac{\partial \phi}{\partial x}|_i + (y_j - y_i)\frac{\partial \phi}{\partial y}|_i + O(h^2), \quad j \in C_i \tag{10}$$

The spatial derivatives are determined by using a weighted least square approximation

$$\min \sum_{j \in C_i} w_{ij}\left(\Delta\phi_{ij} - \Delta x_{ij}\frac{\partial \phi}{\partial x}|_i - \Delta y_{ij}\frac{\partial \phi}{\partial y}|_i\right)^2$$

Where $\Delta\phi_{ij} = \phi_j - \phi_i$, $\Delta x_{ij} = x_j - x_i$ and $\Delta y_{ij} = y_j - y_i$. The w_{is} is a simple inverse distance weighting function and the following form is used in the present paper:

$$w_{ij} = \frac{1}{(\Delta x_{ij}{}^2 + \Delta y_{ij}{}^2)^{1/2}}$$

The solution of this minimization problem leads to a matrix equation according to the principle of the least square fit as follows:

$$\begin{bmatrix} \sum_{j\in C_i} w_{ij}\Delta x_{ij}{}^2 & \sum_{j\in C_i} w_{ij}\Delta x_{ij}\Delta y_{ij} \\ \sum_{j\in C_i} w_{ij}\Delta x_{ij}\Delta y_{ij} & \sum_{j\in C_i} w_{ij}\Delta y_{ij}{}^2 \end{bmatrix} \begin{bmatrix} \frac{\partial \phi}{\partial x}|_i \\ \frac{\partial \phi}{\partial y}|_i \end{bmatrix} = \begin{bmatrix} \sum_{j\in C_i} w_{ij}\Delta x_{ij}(\phi_j - \phi_i) \\ \sum_{j\in C_i} w_{ij}\Delta y_{ij}(\phi_j - \phi_i) \end{bmatrix}$$

The solution of the derivatives can be simply written as the following linear approximation when solving the above equation explicitly:

$$\frac{\partial \phi}{\partial x}|_i = \sum_{j\in C_i} a_{ij}(\phi_j - \phi_i), \quad \frac{\partial \phi}{\partial y}|_i = \sum_{j\in C_i} b_{ij}(\phi_j - \phi_i) \tag{11}$$

Where the coefficients a_{ij} and b_{ij} are defined as the following form:

$$a_{ij} = \frac{\left(\sum_{k=1}^{N} w_{ik}\Delta y_{ik}^2\right) w_{ij}\Delta x_{ij} - \left(\sum_{k=1}^{N} w_{ik}\Delta x_{ik}\Delta y_{ik}\right) w_{ij}\Delta y_{ij}}{\left(\sum_{k=1}^{N} w_{ik}\Delta x_{ik}^2\right)\left(\sum_{k=1}^{N} w_{ik}\Delta y_{ik}^2\right) - \left(\sum_{k=1}^{N} w_{ik}\Delta x_{ik}\Delta y_{ik}\right)^2};$$

$$b_{ij} = \frac{\left(\sum_{k=1}^{N} w_{ik}\Delta x_{ik}^2\right) w_{ij}\Delta y_{ij} - \left(\sum_{k=1}^{N} w_{ik}\Delta x_{ik}\Delta y_{ik}\right) w_{ij}\Delta x_{ij}}{\left(\sum_{k=1}^{N} w_{ik}\Delta x_{ik}^2\right)\left(\sum_{k=1}^{N} w_{ik}\Delta y_{ik}^2\right) - \left(\sum_{k=1}^{N} w_{ik}\Delta x_{ik}\Delta y_{ik}\right)^2}$$

Finally, a semi-discrete form of N-S equations by the least-squares approximation at node i can be obtained as follows:

$$\frac{\partial Q_i}{\partial t} + \sum_{j\in C_i}\{[a_{ij}(f_{ij} - f_i) + b_{ij}(g_{ij} - g_i)] - [a_{ij}(F_{ij} - F_i) + b_{ij}(G_{ij} - G_i)]\} = 0 \tag{12}$$

3.2 Inviscid Fluxes Discretization

According to the idea proposed by Sridar and Balakrishnan [19], the fictitious interface J is built at the midpoint of ray ij, as shown in Fig. 1. The AUSM+-up scheme is used to compute the convection fluxes f_{ij} and g_{ij} as the following form:

$$F_{1/2} = \frac{1}{2}a_{1/2}\left[M_{1/2}(\varphi_J + \varphi_{J+1}) - |M_{1/2}|(\varphi_{J+1} - \varphi_J)\right] + p_{1/2} \tag{13}$$

More details can be found in the work done by Liou

https://doi.org/10.1017/jmech.2017.35 Published online by Cambridge University Press

[20] and Cai *et al*. [9].

3.3 Higher-Order Interpolation

In order to achieve a high order scheme, the Monotonic Upstream-Centered Scheme for Conservation Laws (MUSCL)-type approach with Van Albada limiter, which is often used in finite volume method, is adopted to interpolate the primary variables onto the two sides of the fictitious interface in the present study. The MUSCL reconstruction scheme with a Van Albada limiter can be described as follows:

$$u_{ij}^{+} = u_i + \frac{s_i}{4}\left[(1-ks_i)\Delta_{ij}^{-} + (1+ks_i)(u_j - u_i)\right];$$
$$u_{ij}^{-} = u_j - \frac{s_j}{4}\left[(1-ks_j)\Delta_{ij}^{+} + (1+ks_j)(u_j - u_i)\right] \quad (14)$$

Where

$$\Delta_{ij}^{-} = 2\Delta\vec{r}_{ij} \bullet \nabla u_i - (u_j - u_i), \quad \Delta_{ij}^{+} = 2\Delta\vec{r}_{ij} \bullet \nabla u_j - (u_j - u_i)$$

Here, $\Delta\vec{r}_{ij}$ is the vector pointing from node i to j. The gradient ∇u is computed using equation 15. The limiter s is defined as:

$$s_i = \max\left[0, \frac{2\Delta_{ij}^{-}(u_j - u_i) + \varepsilon}{(\Delta_{ij}^{-})^2 + (u_j - u_i)^2 + \varepsilon}\right];$$
$$s_j = \max\left[0, \frac{2\Delta_{ij}^{+}(u_j - u_i) + \varepsilon}{(\Delta_{ij}^{+})^2 + (u_j - u_i)^2 + \varepsilon}\right]$$

Where ε is a very small positive number for preventing null division, and $\varepsilon = 10^{-12}$ is used in this study. The parameter $\bar{k}$ determines the amount of upwinding, and $\bar{k} = 1/3$ is set in the present work.

3.4 Viscous Flux Discretization

The gradients of the temperature and velocity in the viscous fluxes are calculated using the equation 11. It may be lead to the odd-even decoupling, if the gradient of the interface is calculated by averaging the values of point i and points j, so a correction calculation method of the gradient according to May and Jameson [21] is used in the present work:

$$\nabla\phi_{ij} = \overline{\nabla\phi_{ij}} - \left(\overline{\nabla\phi_{ij}} \bullet \bar{S}_{ij} - \frac{\phi_j - \phi_i}{|\vec{r}_j - \vec{r}_i|}\right)\bar{S}_{ij} \quad (15)$$

Where

$$\overline{\nabla\phi_{ij}} = \frac{1}{2}\left[(\nabla\phi_i) + (\nabla\phi_j)\right], \quad \bar{S}_{ij} = (\vec{r}_j - \vec{r}_i)/(|\vec{r}_j - \vec{r}_i|)$$

This modification leads to a stable discretization of viscous fluxes and does not affect the accuracy. Where solving the High Reynolds number turbulence flows, the $k-\omega$ SST (Shear Stress Transport) is adopted in the present work.

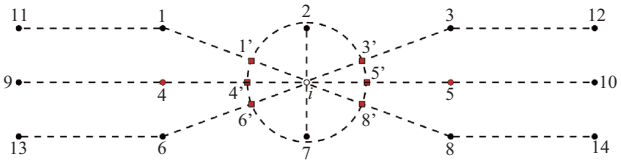


Fig. 2 Illustration for COP reconstruction.

3.5 Temporal Discretization

In the present paper, explicit three-stage Strong Stability Preserving (SSP) Runge-Kutta method is chosen to advance the time evolution. The semi-discrete form of the N-S equations can be written as follows:

$$\frac{\partial Q_i}{\partial t} + R_i = 0 \quad (16)$$

Assuming that the variable Q_i^n is known at time t^n, the solution is advanced over a time step Δt to Q_i^{n+1} at time t^{n+1} by:

$$Q_i^{(1)} = Q_i^n - \Delta t R_i(Q_i^n)$$
$$Q_i^{(2)} = \frac{3}{4}Q_i^n + \frac{1}{4}\left[Q_i^{(1)} - \Delta t R_i(Q_i^{(1)})\right]$$
$$Q_i^{n+1} = \frac{1}{3}Q_i^n + \frac{2}{3}\left[Q_i^{(2)} - \Delta t R_i(Q_i^{(2)})\right]$$

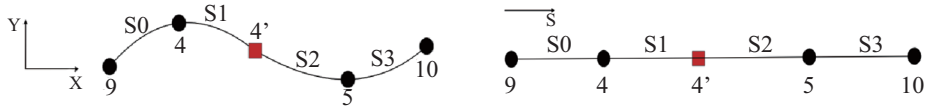
Where Δt represents the time step. In order to accelerate convergence, the local time step and implicit residual smoothing technology is used in the present paper.

4. CLOUD OF POINTS RECONSTRUCTION

The highly anisotropic cloud of points in the viscous boundary layer may lead the least square coefficient matrix to be ill-condition (the condition coefficient number is much larger than 1). Thus, it will be difficult to use least square method to calculate the spatial derivatives accurately. In the present paper, a new method, which is Cloud of Points Reconstruction (COPR), is proposed to reduce the condition coefficient number and the anisotropic cloud of points is repaired to nearly isotropic. The values of the new points are obtained by the Lagrange interpolation, which is used very commonly in engineering applications. As shown in Fig. 2, the new points are 1', 3', 4', 5', 6' and 8'. These points' values are calculated by the Cloud of Points Reconstruction method. Thus the ill conditioned coefficient matrix can be repaired to the healthy state.

The new points are not the original discrete points, so they do not have the value of the flow field. In the present work, the Lagrange interpolation is used to calculate the new points values. Take the new point 4' as an example to describe the COP reconstruction approach. For the Lagrange interpolation approach, at least four points are needed to ensure that the accuracy of interpo-

https://doi.org/10.1017/jmech.2017.35 Published online by Cambridge University Press



(a) Two-dimensional interpolation stencil (b) One-dimensional interpolation stencil

Fig. 3 Illustration for interpolating method.

lation is no less than third order. As shown is Fig. 2, the point 4 and 5 are the original discrete points, and they have the values of the flow field. So other two points (point 9 and point 10) should be found to construct the interpolation stencil. As shown in Fig. 3(a), assuming that point 9 is the point that should be found in "cloud of point" C_4. Then the point 9 should satisfy the following principles:

$$\min(\vec{r}_{49} \bullet \vec{r}_{44'})$$

where $\vec{r}_{49}$ is the unit vector that from point 4 directing to 9. In this way, the point 9 can be found in C_4. Using the same approach, the point 10 can be found in C_5. Thus the two-dimensional interpolation stencil can be constructed as shown in Fig. 3(a).

The two-dimensional stencil can be reduced to one-dimensional by Computing the arc length between the known points, as shown in Fig. 3(b). Then the value of point 4' can be obtained by the Lagrange interpolation polynomial as the following form:

$$L_n(x) = \sum_{i=0}^{n} f(x_i) \prod_{\substack{j=0 \\ j \neq i}}^{n} \frac{x - x_j}{x_i - x_j} \tag{17}$$

5. VALIDATION AND RESULTS

A series of test cases were performed to examine the accuracy and robustness of the present method. Firstly, the gradients of the function, which have the analytical gradients, are calculated based on the anisotropic cloud of points. Secondly, the laminar viscous flows and turbulence flows around NACA0012 are simulated using the proposed meshfree method.

5.1 Case 1 The Function with Analytical Gradients

The functions are $f_1 = \sin(\pi x)\cos(\pi y)$ and $f_2 = x^3 y^2 + x^2$. The analytical gradients of the two functions are

$$\begin{aligned} \partial f_1 / \partial x &= \cos(\pi x)\cos(\pi y)\pi \\ \partial f_1 / \partial y &= -\sin(\pi x)\sin(\pi y)\pi \end{aligned} \quad \text{and} \quad \begin{aligned} \partial f_2 / \partial x &= 3x^2 y^2 + 2x \\ \partial f_2 / \partial y &= 2x^3 y \end{aligned}$$

The distribution of the high anisotropic cloud of points is shown in Fig. 4. The points distribution is 101 × 2001 based on the computational domain $x \times y = 1 \times 1$. The cloud of points will be high anisotropic when the minimum normal space is 10^{-6} for that the cloud of point

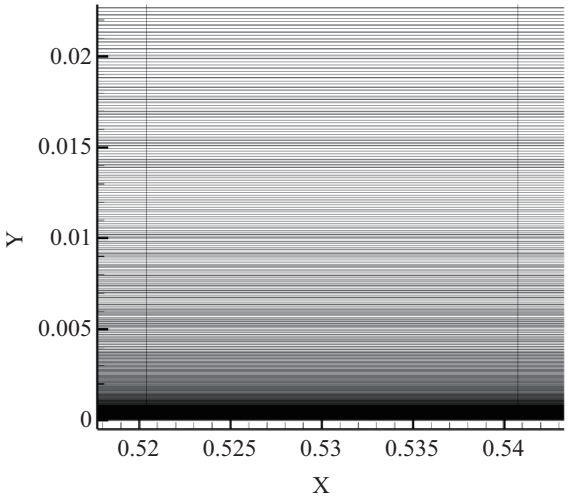


Fig. 4 The high anisotropic cloud of points distribution.

will be highly anisotropic.

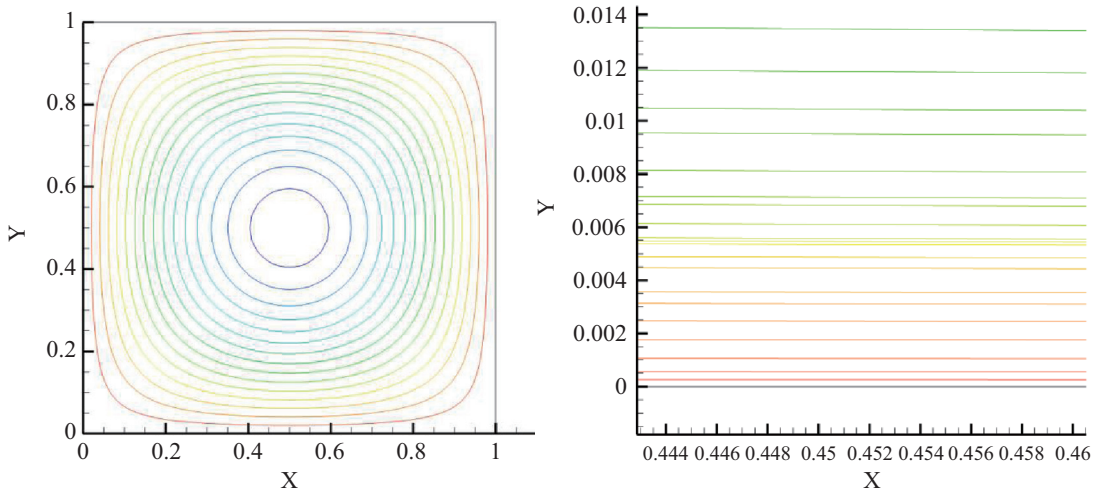
The gradients of the function f_1 and f_2 are calculated using the conventional least square method and the proposed least square method with COPR. The simulated results are compared with the analytical gradients. Both the simulation results of $\partial f/\partial x$ and $\partial f/\partial y$ can give the same conclusion, but only the results of $\partial f/\partial y$ is given arbitrarily in Fig. 5 and Fig. 6. It can be seen from the figures that the results with no COPR in the high anisotropic cloud of points area show the great volatility. While the COPR method show a better results

The distribution of $\partial f/\partial y$ at x = 0.5 is shown in Fig. 7 and Fig. 8. It can be seen from the figures that the gradients calculated by the conventional least square method (with no COPR) in the high anisotropic cloud of points region give the obvious error where compared with the analytical solutions, while the least square method based on the COPR method give much better results and agree well with the analytical solutions. This means that it will be difficult to use the conventional least square meshfree method to calculate the spatial derivatives accurately. On the other hand, it can be illustrated that the COPR method can improve the high anisotropic cloud of points to be nearly isotropic and give the accuracy and ability of fitting the derivatives.

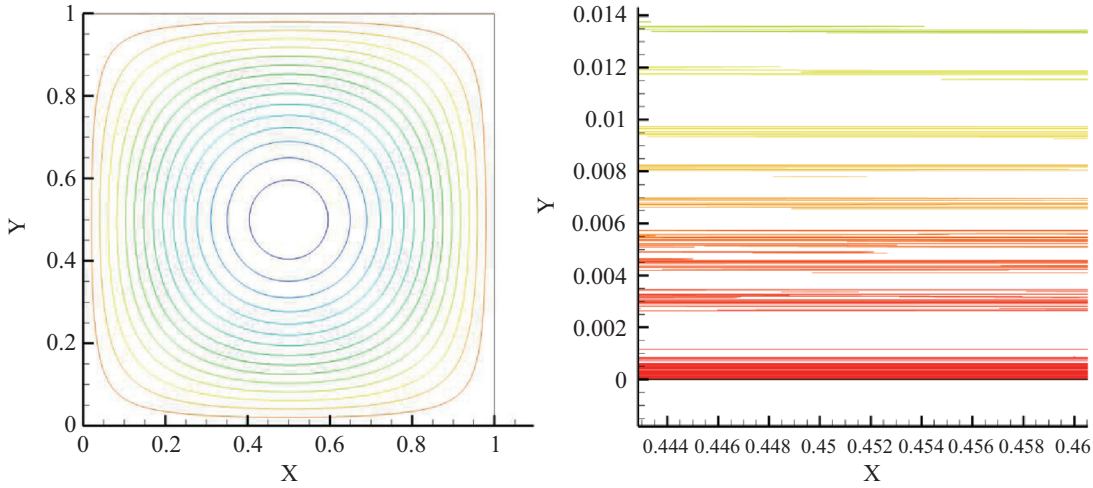
5.2 Case 2 The Laminar Flows Around NACA0012 Airfoil

In order to validate the accuracy and robustness of the COPR meshfree method proposed in the present paper, the laminar viscous flows around NACA0012 airfoil

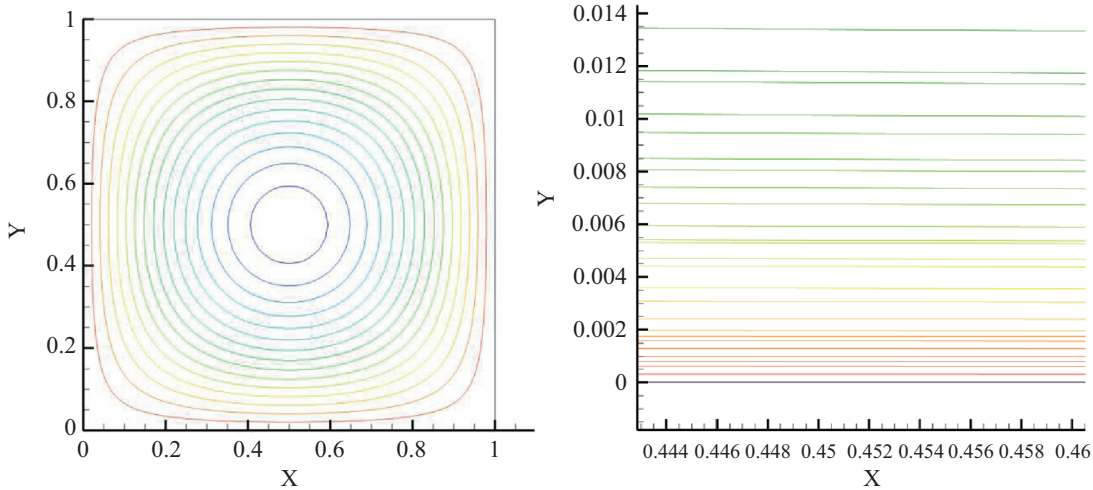
https://doi.org/10.1017/jmech.2017.35 Published online by Cambridge University Press



(a) Analytical result (left is all domain, right is bottom area)



(b) Numerical result with no COP reconstruction (left is all domain, right is bottom area)



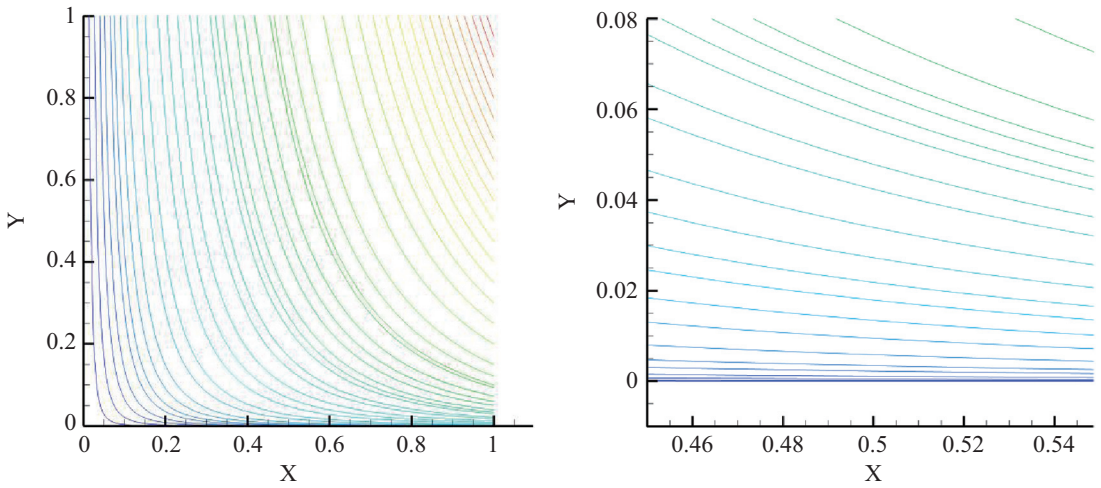
(c) Numerical result with COP reconstruction (left is all domain, right is bottom area)

Fig . 5 The distribution for gradient $\partial f_1/\partial y$.

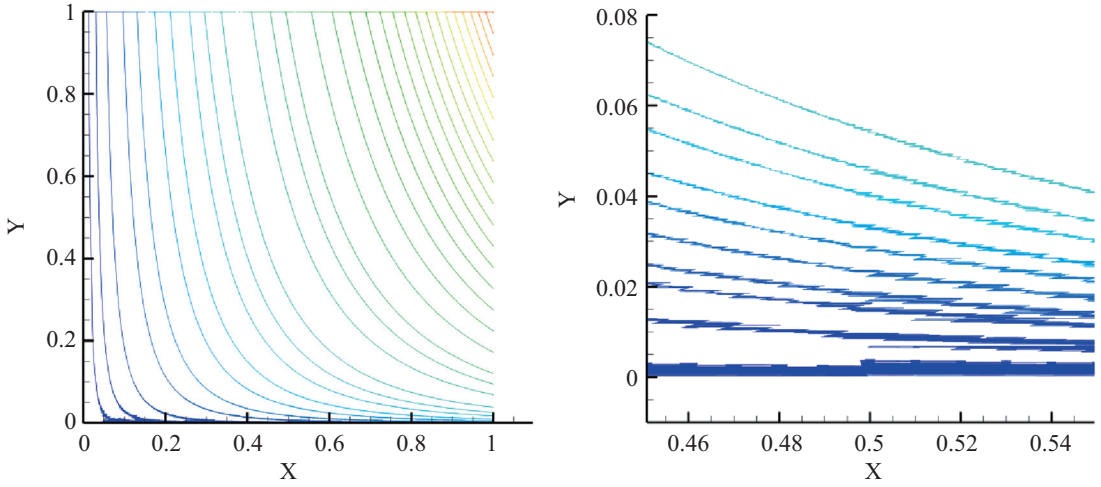
were simulated in this section. The cloud of points distribution for NACA0012 airfoil computational domain is shown as Fig. 9. The far field boundaries were placed about 20 chord lengths of the downstream, upstream and both side of the airfoil. The normal placement of the first point off the wall is 1.0×10^{-6} times of the airfoil chord, which results in an average y+ value of less than 1.0. Total 23985 points with 260 points lying on the airfoil surface were placed on the computational domain.

The free stream conditions in the present computation

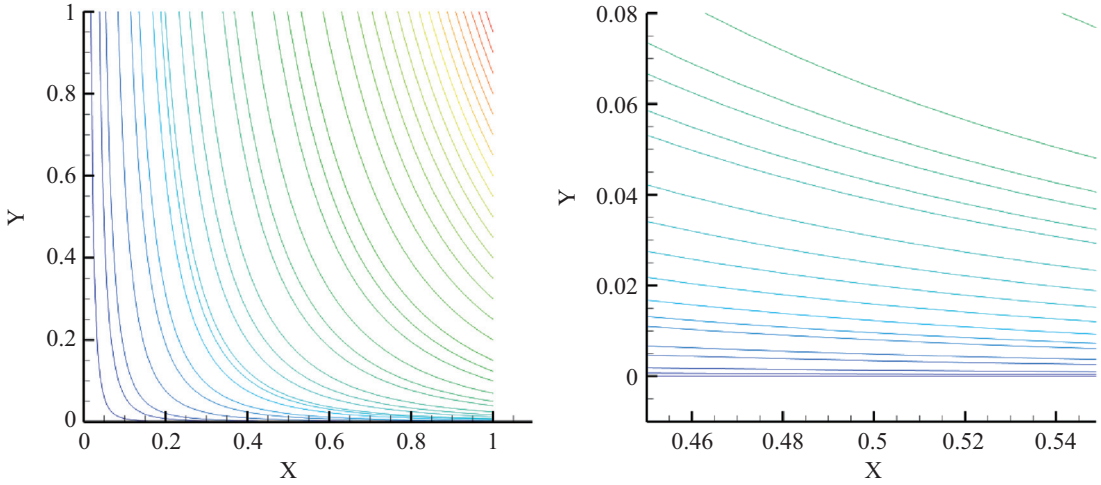
https://doi.org/10.1017/jmech.2017.35 Published online by Cambridge University Press



(a) Analytical result (left is all domain, right is bottom area)



(b) Numerical result with no COP reconstruction (left is all domain, right is bottom area)



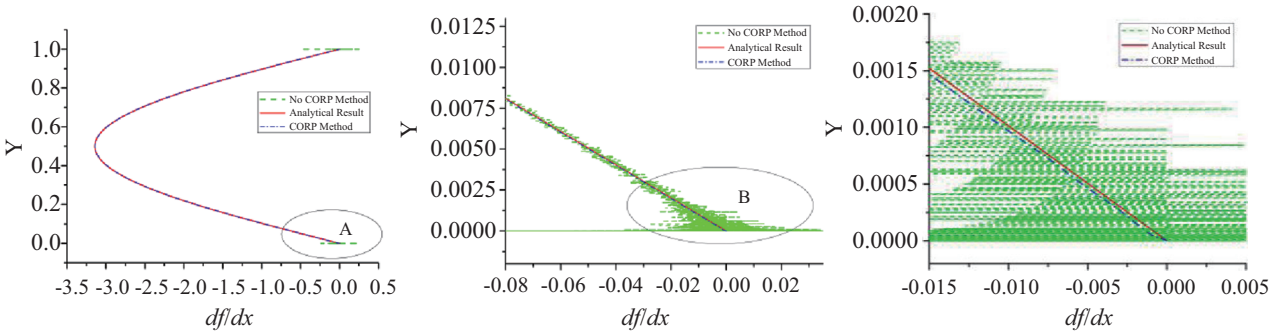
(c) Numerical result with COP reconstruction (left is all domain, right is bottom area)

Fig. 6 The distribution for gradient $\partial f_1/\partial y$.

are the following: Case (a): Ma = 0.5, $\alpha = 0°$, $Re_\infty = 5000$ and Case (b): Ma = 0.8, $\alpha = 10°$, $Re_\infty = 500$.

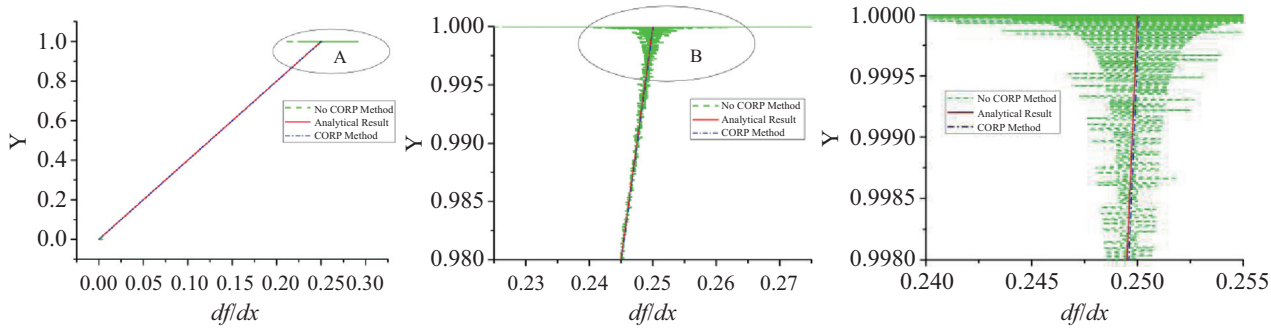
The first test case (a) is a difficult test problem for the Reynolds number is near the upper limit for the steady laminar flow. It means that the Reynolds number is very high for the laminar viscous flow. This flow was simulated by the conventional least square meshfree method and the proposed meshfree method based on COP reconstruction, respectively. Figure 10 gives the streamline near the trailing edge of the airfoil. Figure 10(a) is the results for conventional least-squares meshfree method, Fig. 10(b) is the results obtained by the pro-

https://doi.org/10.1017/jmech.2017.35 Published online by Cambridge University Press



(a) x = 0.5 (b) Bottom area A (c) Bottom area B

Fig. 7 The distribution of $\partial f_1/\partial y$ at x = 0.5.



(a) x = 0.5 (b) Top area A (c) Top area B

Fig. 8 The distribution of $\partial f_2/\partial y$ at x=0.5.

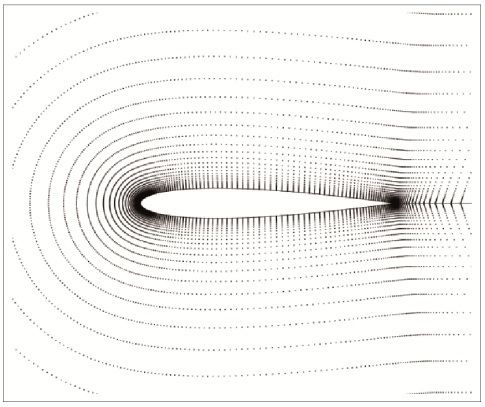
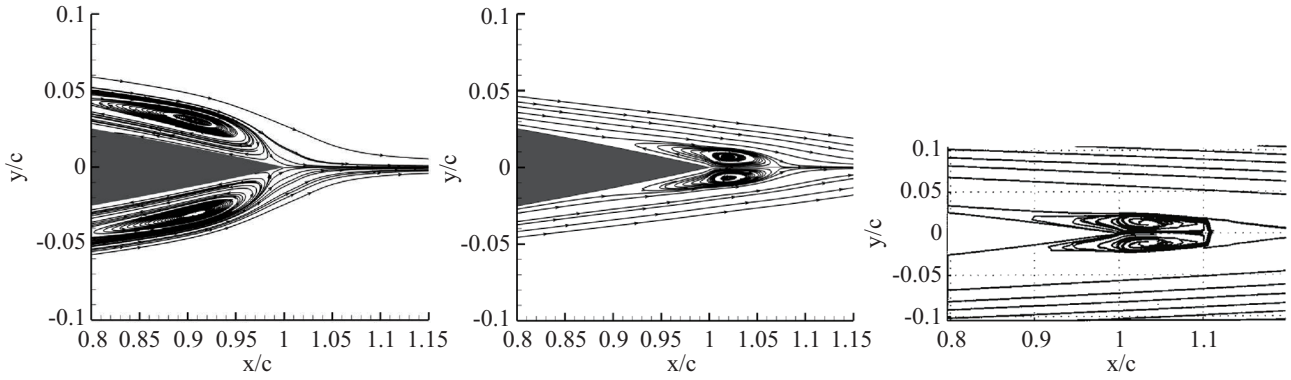


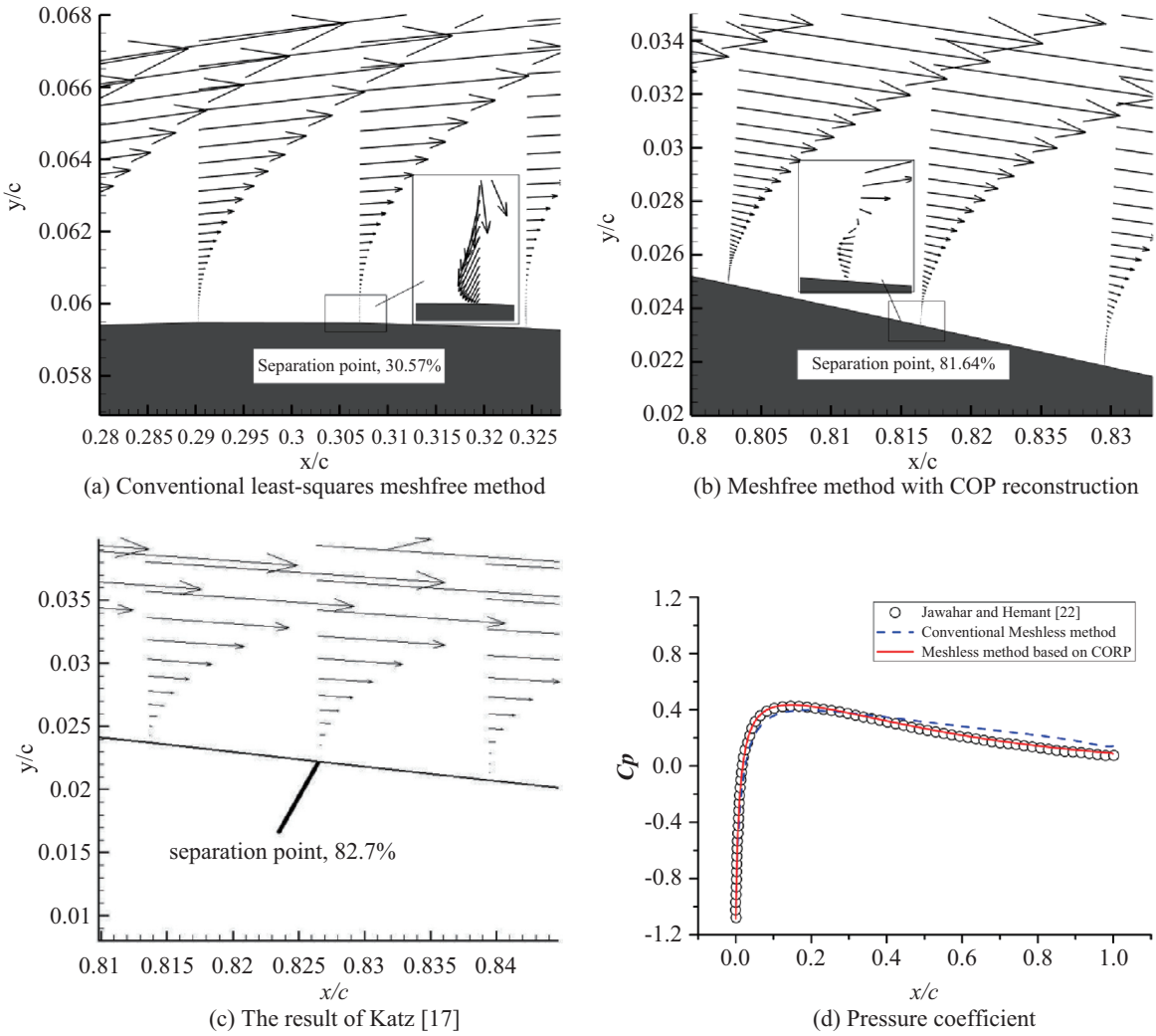
Fig. 9 The point distribution of the computational domain.



(a) Conventional least-squares meshfree method (b) Meshfree method with COP reconstruction (c) The result of Jawahar and Hemant [22]

Fig. 10 Comparison of streamlines near the trailing edge for Ma = 0.5, α = 0°, Re_∞ = 5000.

https://doi.org/10.1017/jmech.2017.35 Published online by Cambridge University Press



(a) Conventional least-squares meshfree method

(b) Meshfree method with COP reconstruction

(c) The result of Katz [17]

(d) Pressure coefficient

Fig. 11 Comparison of Separation point and pressure coefficient for Ma = 0.5, $\alpha = 0°$, $Re_\infty = 5000$.

posed meshfree method with COP reconstruction. The results shown in Fig. 10(c) is obtained by Jawahar and Hemant [22] using the finite volume method. The vortex center position obtained by the conventional meshfree method is located at 90%*c*, while the location given by present meshfree method with COP reconstruction is very close to the result of Jawahar, which is about 102%*c*. It also can be seen from Fig. 10 that the proposed method gives more symmetrical vortices on either side of the $y = 0$ axis when compared with Jawahar's results.

Figure 11 shows the comparison of the separation point. Due the viscosity and adverse pressure gradient, the flow is separated on the airfoil surface. The range of the separation point predicted by Mavriplis *et al* [23] is about 80.9%-83.4%. The proposed meshfree method performs extremely well at predicting separation point compared with the results of Mavriplis. The predicted separation point at 81.64% is also very close to the prediction of Katz and Jameson [17], which is shown in Fig. 11(c). The conventional least square meshfree method gives very poor prediction and it also can be said that the location of the separation point is wrong. The pressure coefficient distribution around the airfoil surface is shown in Fig. 11(d). The meshfree method based on COP reconstruction performs well compared with pressure coefficient distribution of Jawahar, while the conventional meshfree method gives unsatisfactory results.

The second test example, for the flow Ma = 0.8, $\alpha = 10°$, $Re_\infty = 500$ past the NACA0012 airfoil, is a low-Reynolds-number flow, which has a large separated region on the upper surface of the airfoil. The objective is to demonstrate the ability of the new proposed meshfree method with COP reconstruction to accurately simulate this complex flow feature based on the high anisotropic cloud of points.

The prominent vortex extending over 50% of the chord on the upper surface, which is the main feature of this flow, is clearly shown in Fig. 12. The results obtained by the COP reconstruction meshfree method agrees well with the result of Jawahar and Hemant [22], while the meshfree method without COP reconstruction does not compare well with the solution of Jawahar. The surface pressure coefficient distribution is shown in Fig. 12(d). Obviously, the COP reconstruction method gives better results than the meshfree method without COP reconstruction when compared with the solution of Jawahar. It is evident from the simulation solutions that the proposed meshfree method in the present paper can

https://doi.org/10.1017/jmech.2017.35 Published online by Cambridge University Press

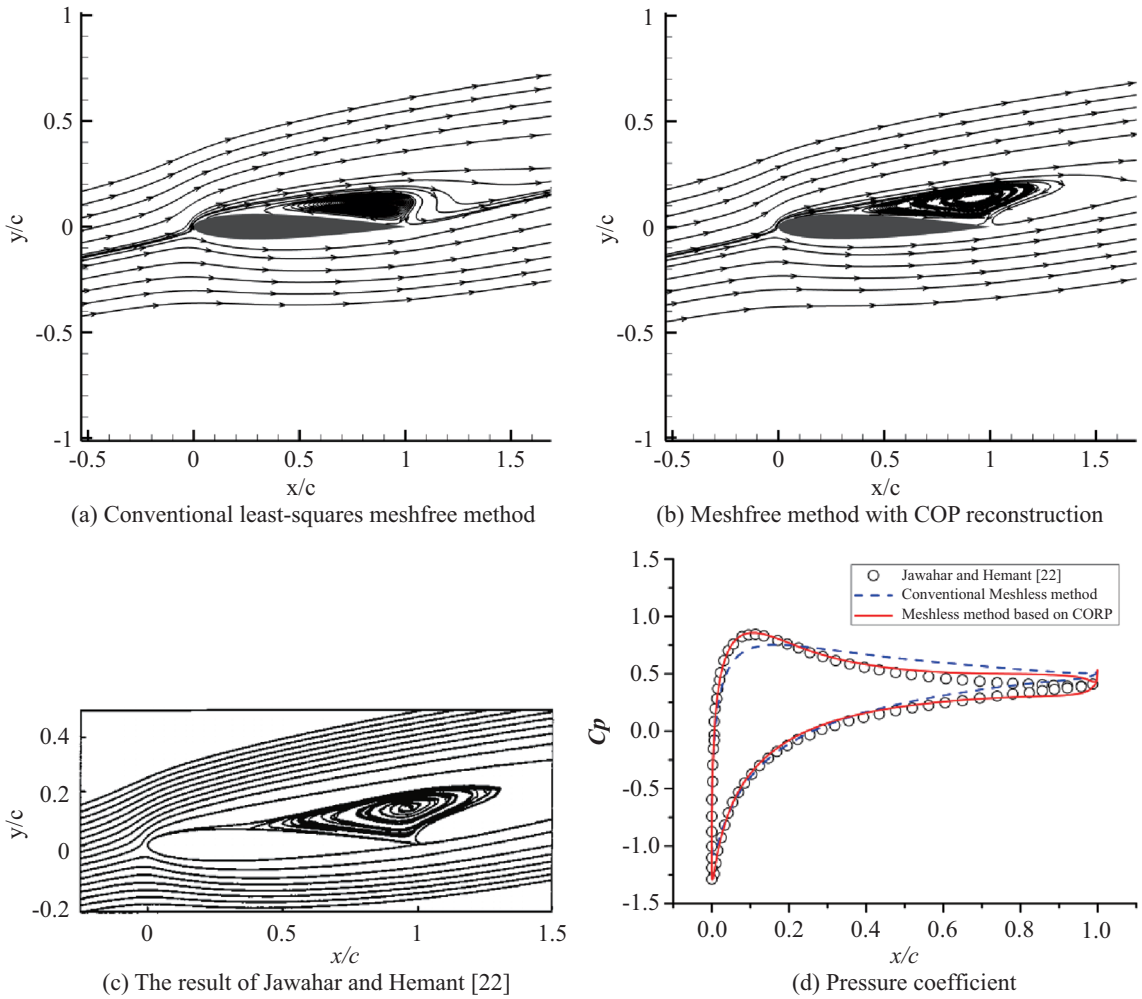


Fig. 12 Comparison of streamlines and pressure coefficient for Ma = 0.8, $\alpha = 10°$, $Re_\infty = 500$.

accurately predict the laminar viscous flows.

5.3 Case 3 The Turbulence Flows Around NACA0012

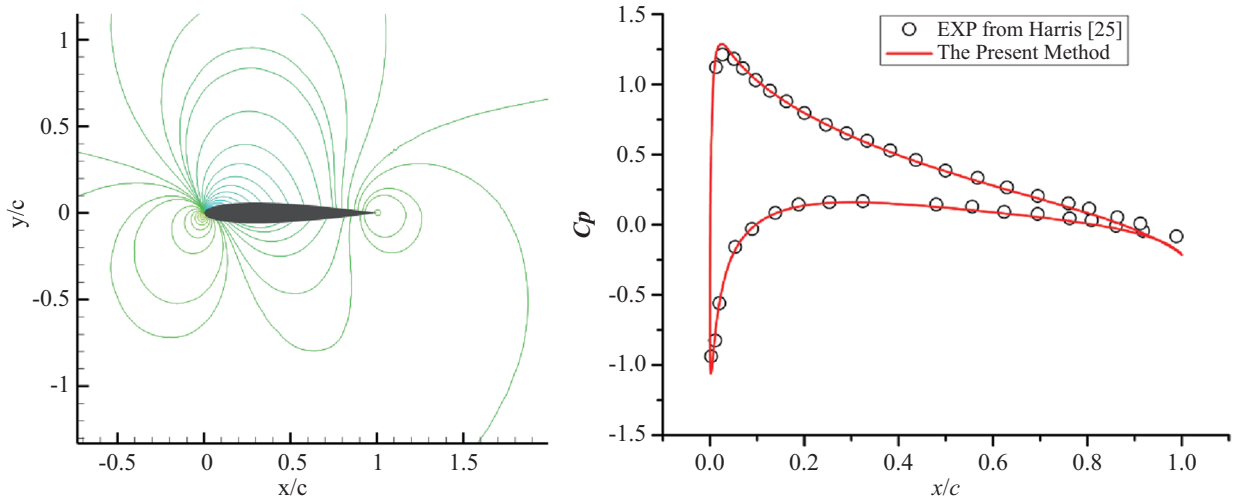
To further demonstrate the capabilities of the proposed COP reconstruction method, some complex turbulent flows, including a subsonic turbulent flow and a transonic turbulent flow, past NACA0012 have been chosen for simulating. The turbulent model adopted in the present paper is the $k - \omega$ SST (Shear Stress Transport) model. More details about this turbulent model can be found in the literature [24]. The free stream conditions for the turbulent flows in the present computation are the following: Case(c): Ma = 0.5, $\alpha = 3.51°$, $Re_\infty = 2.93 \times 106$ and Case (d): Ma = 0.799, $\alpha = 2.26°$, $Re_\infty = 9.0 \times 106$.

The first turbulent test case is for the subsonic flow Ma = 0.5, $\alpha = 3.51°$, $Re_\infty = 2.93 \times 106$ past NACA0012. This test case is chosen to demonstrate the efficacy of the COP reconstruction method in handing the subsonic turbulent flows. The pressure contours displayed in Fig. 13(a) clearly shows the reasonable flow field around the NACA0012 airfoil. Computed pressure coefficient distribution compares well with the experimental data [25], which is shown in Fig. 13(b).

The second turbulent test case is one of the most challenging cases for turbulent models in terms of capturing shock location and predicting the variation after shock. This test case corresponds to simulating transonic turbulent flow over NACA0012 airfoil with angle of attack of 2.26°, freestream Mach number 0.799 and Reynolds number 2.93 × 106. Furthermore, the $k - \omega$ SST (Shear Stress Transport) model is chosen to predict this complex shock-induced separation flow.

In this turbulent flow, the adverse pressure gradient caused by the shock-boundary layer interaction leads to a flow separation after the shock on the upper side airfoil. The aft-shock separation bubble simulated by the proposed turbulent meshfree solver is clearly shown in Fig. 14. The computed iso-pressure contours around the airfoil are shown in Fig. 15(a). It can be seen from the counters that the shock is located at about 50% of the chord on the upper surface. The variation of the surface pressure coefficient in comparison to the experimental data measured by Harris [25] is shown in Fig. 15(b). An excellent agreement is obtained and the shock is captured at right location. The well simulated turbulent results indicate that the proposed meshfree method with COP reconstruction coupled with $k - \omega$ SST model can accurately capture the characteristics of the turbulent flows past NACA0012 airfoil.

https://doi.org/10.1017/jmech.2017.35 Published online by Cambridge University Press



(a) Pressure contours (b) Pressure coefficient

Fig. 13 Subsonic turbulent flow (Ma = 0.5, α = 3.51°, Re_∞ = 2.93 × 106).

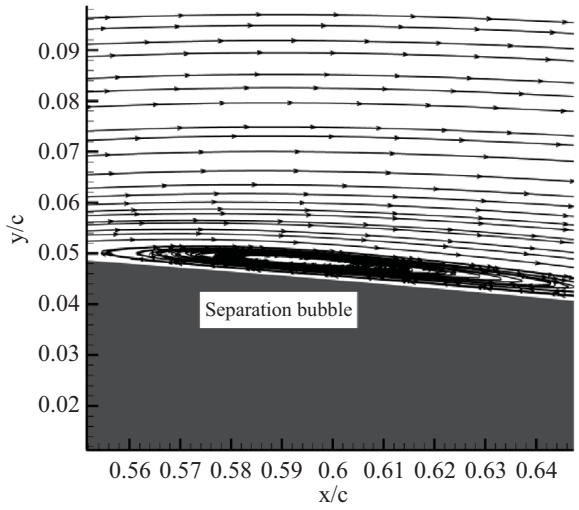
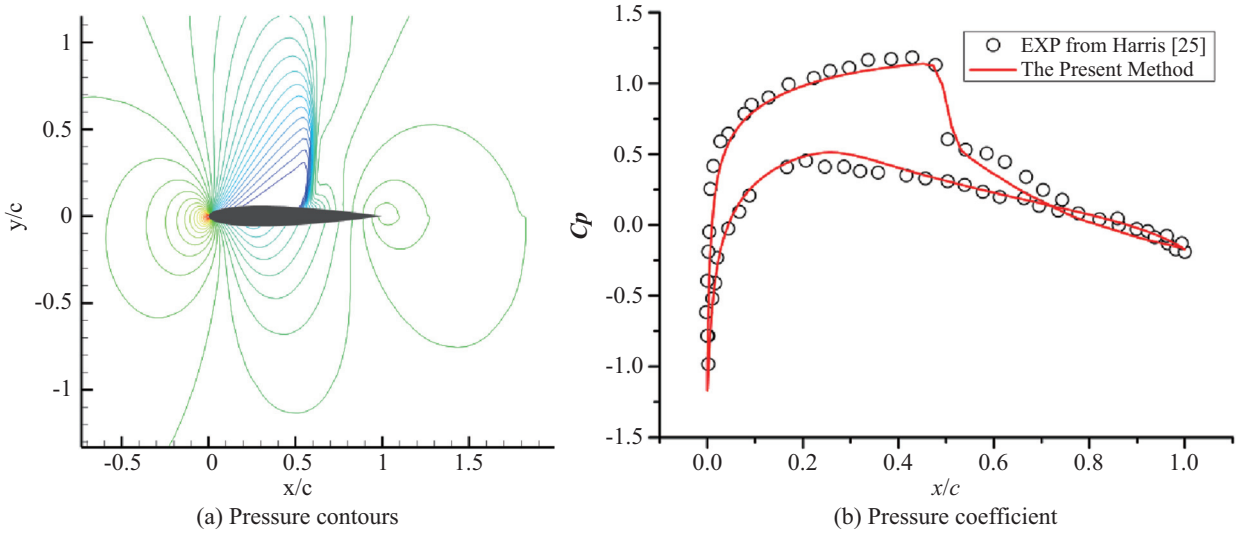


Fig. 14 Separation bubble (Ma = 0.799, α = 2.26°, Re_∞ = 9.0 × 106).



(a) Pressure contours (b) Pressure coefficient

Fig. 15 Transonic turbulent flow (Ma = 0.799, α = 2.26°, Re_∞ = 9.0 × 106).

https://doi.org/10.1017/jmech.2017.35 Published online by Cambridge University Press

6. CONCLUSIONS

The present paper provides a new numerical method for solving the compressible Navier-Stokes and Reynolds-average Navier-Stokes equations within the framework of meshfree solver. Some laminar and turbulent flows past NACA0012 airfoil were simulated using the proposed method in the present work. The proposed COP reconstruction method is suitable for extending the conventional least square meshfree method to compute complex viscous flows, including laminar flows and turbulent flows, in high anisotropic cloud of points structure. The novelty of the presented method lies the fact that the high anisotropic cloud of points can be repair to nearly isotropic cloud of points. So the spatial derivative can be solved by the least square method accurately. The results computed have been compared with the classical finite volume method data (for laminar flows) and previous experimental data (for turbulent flows). The good agreement with the reference data validates the accuracy and robustness of the proposed meshfree method. Also, to the best of the authors' knowledge, this basic idea happens to be the first proposed by the authors' group for the framework of meshfree solvers. Presently the authors are involved in extending this idea to some more complex unsteady flows and 3D simulations.

ACKNOWLEDGEMENTS

This research has been supported by the [National Natural Science Foundation of China] under Grant [number 11072114]; and [Science and Technology Innovation Foundation of Shanghai Aerospace] under Grant [number SAST201365].

REFERENCES

1. Lucy, L. B., "A Numerical Approach to the Testing of the Fission Hypothesis," *The Astronomical Journal*, **82**, pp. 1013-1024 (1977).
2. Liu, G. R., *Mesh Free Method: Moving Beyond the Finite Element Method*, CRC Press, Boca Raton (2003).
3. Liu, G. R. and Gu, Y. T., *An Introduction to Meshfree Methods and Their Programming*, Springer, Berlin (2005).
4. Liszka, T. and Orkisz, J., "The Finite Difference Method at Arbitrary Irregular Grids and Its Application in Applied Mechanics," *Computers and Structures*, **11**, pp. 83-95 (1980).
5. Batina, J. T., "A Grid-Free Euler/Navier-Stokes Solution Algorithm for Complex Aircraft Applications," *31st Aerospace Sciences Meeting*, U.S. (1993).
6. Deshpande, S. M., Ghosh, A. K. and Mandal, J. C., "Least Squares Weak Upwind Methods for Euler Equations," *Fluid Mechanics Report*, **No. FM4**, Department of Aerospace Engineering, Indian Institute of Science (1989).
7. Ghosh, A. K. and Deshpande, S. M., "Least Squares Kinetic Method for Inviscid Compressible Flows," *12th Computational Fluid Dynamics Conference*, U.S. (1995).
8. Dauhoo, M. Z., Ghosh, A. K., Ramesh, V. and Deshpande, S. M., "q-LSKUM-A New Higher-Order Kinetic Upwind Method for Euler Equations Using Entropy Variables," *Computational Fluid Dynamics Journal*, **9**, pp. 272-77 (2000).
9. Cai, X. W. *et al.*, "Application of Hybrid Cartesian Grid and Gridless Approach to Moving Boundary Flow Problems," *International Journal For Numerical Methods in Fluids*, **72**, pp. 994-1013 (2013).
10. Katz, A. J., "Gridless Methods for Computational Fluid Dynamics," PH.D. Dissertation, Department of Aeronautics and Astronautics, Stanford University, California, U.S.A. (2009).
11. Morinishi K., "An Implicit Gridless Type Solver for the Navier-Stokes Equations," *Computational Fluid Dynamics Journal*, **9**, pp. 551-560 (2000).
12. Liu, G. R. and Xu, G. X., "A Gradient Smoothing Method (GSM) for Fluid Dynamics Problems," *International Journal For Numerical Methods In Fluids*, **58**, pp. 1101-1133(2008).
13. Yao, J. Y. *et al*., "A Moving-Mesh Gradient Smoothing Method for Compressible CFD Problems, " *Mathematical Models & Methods in Applied Sciences*, **23**, pp. 273-305 (2013).
14. Munikrishna, N. and Balakrishnan, N. "Turbulent Flow Computations on a Hybrid Cartesian Point Distribution Using Meshless Solver LSFD-U," *Computers & Fluids*, **40**, pp. 118-138 (2011).
15. Namvar, M. and Jahangirian, A. "An Investigation of Mesh-Less Calculation for Compressible Turbulent Flows," *Computers & Fluids*, **86**, pp. 483-489 (2013).
16. Su, X. R., Yamamoto, S. and Nakahashi, K., "Analysis of a Meshless Solver for High Reynolds Number Flow," *International Journal for Numerical Methods in Fluids*, **72**, pp. 505-527 (2013).
17. Katz, A. and Jameson, A., "Edge-Based Meshless Methods for Compressible Viscous Flow with Applications to Overset Grids," *AIAA paper 2008-3989, AIAA 38th Fluid Dynamics Conference*, Seattle, WA, (2008).
18. Kennett, D. J. *et al*., "An Implicit Meshless Method for Application in Computational Fluid Dynamics," *International Journal for Numerical Methods in Fluids*, **71**, pp. 1007-1028 (2013).
19. Sridar, D. and Balakrishnan, N., "An Upwind Finite Difference Scheme for Meshless Solver," *Journal of Computational Physics*, **189**, pp. 1-29 (2003).
20. Liou, M. S., "A Sequel to AUSM, Part Ⅱ :

https://doi.org/10.1017/jmech.2017.35 Published online by Cambridge University Press

AUSM+-up for all Speeds," *Journal of Computational Physics*, **214**, pp. 137-170 (2006).

21. May, G. and Jameson, A. "Unstructured Algorithm for Inviscid and Viscous Flows Embedded in a Unified Solver Architecture: Flo3xx," *43rd AIAA Aerospace Sciences Meeting and Exhibit*, U.S. (2005).
22. Jawahar, P. and Hemant, K., "A High-Resolution Procedure for Euler and Navier-Stokes Computations on Unstructured Grids," *Journal of Computational Physics*, **164**, pp. 165-203 (2000).
23. Mavriplis, D., Jameson, A. and Martinelli, L., "Multigrid Solution of the Navier-Stokes Equations on Triangular Meshes," *AIAA paper 89-0120, AIAA 27th Aerospace Sciences Meeting*, Reno, NV (1989).
24. Menter, F. R., "Two-Equation Eddy-Viscosity Turbulence Models for Engineering Applications," *AIAA Journal*, **32**, pp. 269-289 (1994).
25. Harris, C. D., "Two-Dimensional Aerodynamic Characteristics of the NACA0012 Airfoil in the Langley 8-foot Transonic Pressure Tunnel," *NASA-TM-81927*, NASA Langley Research Center; Hampton, VA, U.S. (1981).

(Manuscript received November 17, 2016,
accepted for publication April 24, 2017.)

https://doi.org/10.1017/jmech.2017.35 Published online by Cambridge University Press